Microporous and Mesoporous Materials 266 (2018) 214–222

Contents lists available at ScienceDirect

Microporous and Mesoporous Materials

journal homepage: www.elsevier.com/locate/micromeso

Synergistic effects of inter- and intra-particle porosity of TiO_2 nanoparticles on photovoltaic performance of dye-sensitized solar cells

Ji Young Ahn[a], Xiuting Luo[b], Soo Hyung Kim[a,b,*]

[a] Research Center for Energy Convergence Technology, Pusan National University, 2, Busandaehak-ro 63beon-gil, Geumjeong-gu, Busan, 46241, Republic of Korea
[b] Departments of Nano Fusion Technology and Nanoenergy Engineering, Pusan National University, 2, Busandaehak-ro 63beon-gil, Geumjeong-gu, Busan, 46241, Republic of Korea

ARTICLE INFO

Keywords:
inter-particle porosity
Intra-particle porosity
TiO_2 nanoparticles
Photoactive layer
Dye-sensitized solar cells

ABSTRACT

We investigated the effects of the inter- and intra-particle porosity of TiO_2 nanoparticles (NPs) on the resulting photovoltaic performance of DSSCs. Solid and porous TiO_2 NPs with controlled intra-particle porosity were fabricated using Brij-58-templated aerosol-gel and calcination processes. The fabricated solid and porous TiO_2 NPs were stacked as thin films with inter-particle porosity using ethyl cellulose-templated screen-printing and calcination processes. Controlling the inter-particle porosity of TiO_2 NPs was found to be much more effective than controlling the intra-particle porosity of TiO_2 NPs for supporting the maximization of the number of dye molecules. The DSSCs composed of porous photoactive layer with porous TiO_2 NPs were found to have the best power conversion efficiency. This suggests that the TiO_2 NPs with porous structures, due to the controlled formation of both inter- and intra-particle porosity, can maximize the light harvesting of DSSCs through better dye adsorption and effective light trapping.

1. Introduction

Since dye-sensitized solar cells (DSSCs) were first reported by Grätzel et al. DSSCs have been regarded as a promising candidate for next-generation solar cells because of their inexpensive and simple manufacturing and relatively high power conversion efficiency (PCE) [1]. DSSCs are mainly composed of a semiconductor nanocrystalline film covered with a molecular dye layer, a redox couple in a liquid electrolyte, and a platinum-based transparent conducting oxide electrode [2,3]. To improve the overall PCE of DSSCs, many researchers have concentrated on the TiO_2-based semiconductor nanocrystalline layer, for which they have developed new types of dyes with the goal of reducing the interfacial resistances so that the generation and transfer of photo-induced electrons at the TiO_2/dye/electrolyte interfaces can be improved when they are irradiated by sunlight [4–10]. However, to increase the PCE of DSSCs, it is necessary to increase the initial amount of dye adsorbed onto the surface of the TiO_2 particles accumulated on the photoactive layer (PL) of the DSSCs. Many research groups have reported on successful means of increasing the amount of dye adsorption by employing micro- and nano-structured TiO_2 [11–16].

Maldonado-Valdivia et al. (2013) examined the effects of several surfactants (e.g., Triton X-100, polyethylene glycol, and ethyl cellulose (EC)) on the formation of porous TiO_2 for the PL of DSSCs. They observed that the inter-particle porosity of a TiO_2 thin film was related to the type and quantity of the surfactant templates added during the preparation of a TiO_2 paste. Among the surfactants, EC was found to be useful for realizing the inter-particle porosity of a TiO_2 nanoparticle (NP)-accumulated thin film for the PL of DSSCs. This is because EC exhibits a more complex molecular structure than other surfactants so that a solid TiO_2-accumulated PL with a very high inter-particle porosity could be successfully fabricated for DSSCs [17]. Byun et al. (2004) employed CTAB as a template for the $TiCl_4$ precursor to fabricate a TiO_2 NP-accumulated thin film with inter-particle porosity. Briefly, a $TiCl_4$ solution was dropped onto the surface of an FTO glass substrate, after which it was dipped into a CTAB-dispersed aqueous solution for 36–72 h. The resulting PCE of the DSSC composed of TiO_2 with inter-particle porosity, formed using CTAB, was around 2.2%, while that of the DSSC formed without CTAB was around 1% [18]. Unlike previous studies, Latini et al. (2015) examined the effects of a range of surfactants on the formation of intra-particle pores for the TiO_2 NPs for DSSCs. They employed SiO_2 NPs as the hard template and pluronic P123/Brij-58 as the soft template. The resulting PCE of the DSSCs employing TiO_2 NP with P123-templated intra-particle porosity was found to be around 6.8%, which was 19.3% greater than the PCE of

* Corresponding author. Research Center for Energy Convergence Technology, Pusan National University, 2, Busandaehak-ro 63beon-gil, Geumjeong-gu, Busan, 46241, Republic of Korea.
E-mail address: sookim@pusan.ac.kr (S.H. Kim).

https://doi.org/10.1016/j.micromeso.2018.03.003
Received 26 October 2017; Received in revised form 4 March 2018; Accepted 6 March 2018
Available online 07 March 2018
1387-1811/

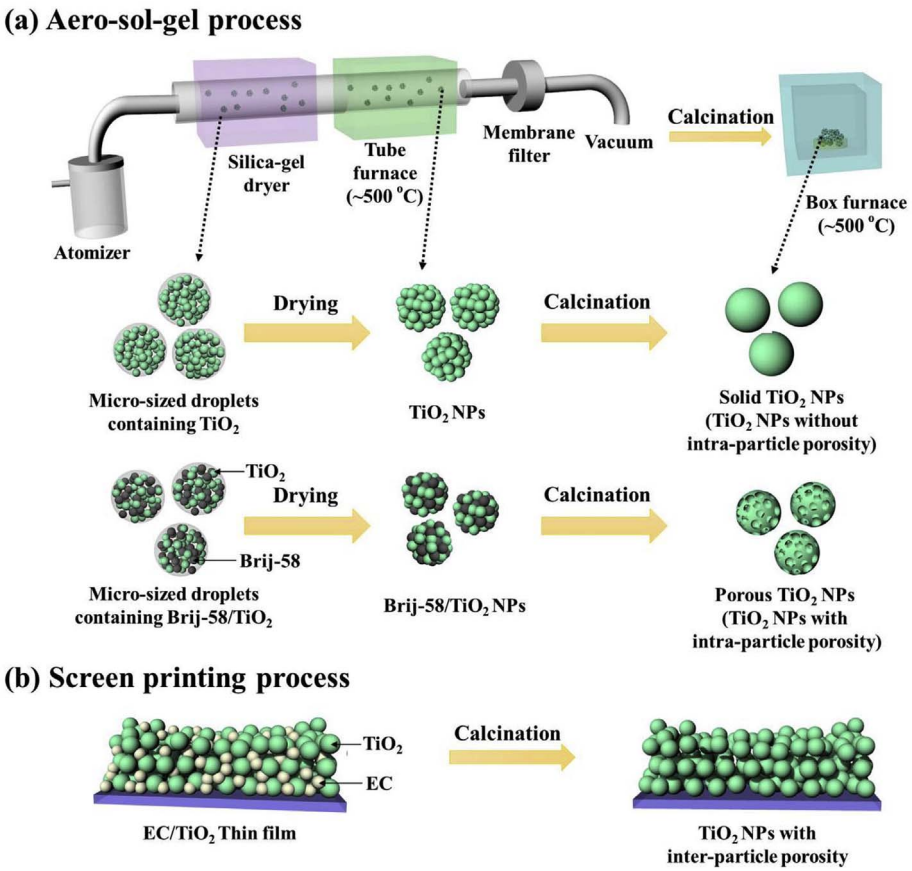

Fig. 1. Schematic of fabrication of TiO_2 NPs with (a) intra-particle porosity using aerosol-gel and subsequent calcination processes and (b) inter-particle porosity using screen printing and subsequent calcination processes.

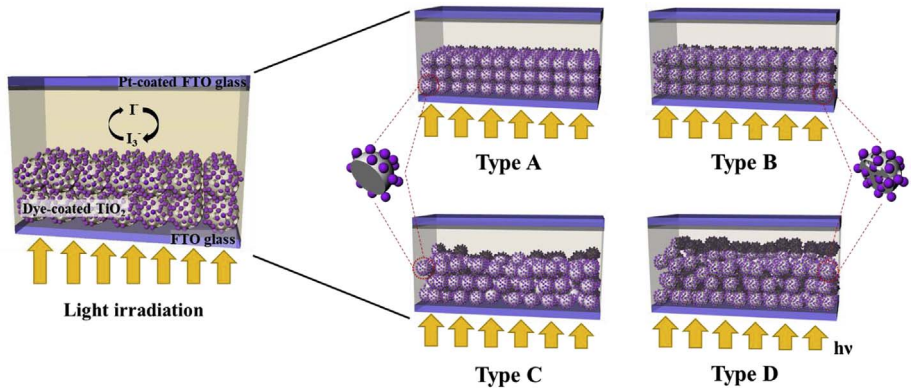

Fig. 2. Schematic of different types of DSSCs; (a) Type A: solid PL with solid TiO_2 NPs, (b) Type B: solid PL with porous TiO_2 NPs (intra-particle porosity), (c) Type C: porous PL with solid TiO_2 NPs (inter-particle porosity), (d) Type D: porous PL with porous TiO_2 NPs (both inter- and intra-particle porosity).

around 5.7% for those DSSCs with SiO_2-templated TiO_2 NPs. However, their approach, which was based on beaker chemistry, had a major disadvantage of requiring 1–7 days or even more to fabricate the TiO_2 NPs with intra-particle porosity [19].

Numerous research groups have reported that tuning either the inter- or intra-particle porosity of TiO_2 NPs accumulated in the PLs can strongly affect the photovoltaic performance of DSSCs [18–22]. However, to the best of our knowledge, the effects of both the inter- and intra-particle porosity of TiO_2 NPs on the photovoltaic performance of DSSCs have not yet been systematically explored yet. Therefore, we set out to investigate the synergistic effects of the inter- and intra-particle porosity of TiO_2 NPs on the photovoltaic performance of DSSCs in terms of the amount of dye molecules adsorbed, open-circuit voltage (V_{oc}), short-circuit current density (J_{sc}), fill factor (*FF*), and PCE. Specifically, to control the intra-particle porosity of TiO_2 NPs, we employed a relatively simple, rapid, and viable Brij-58 surfactant-templated aerosol-gel method. Porous TiO_2 NPs with various intra-particle porosities can provide controlled SSA so that the initial concentration of adsorbed dye

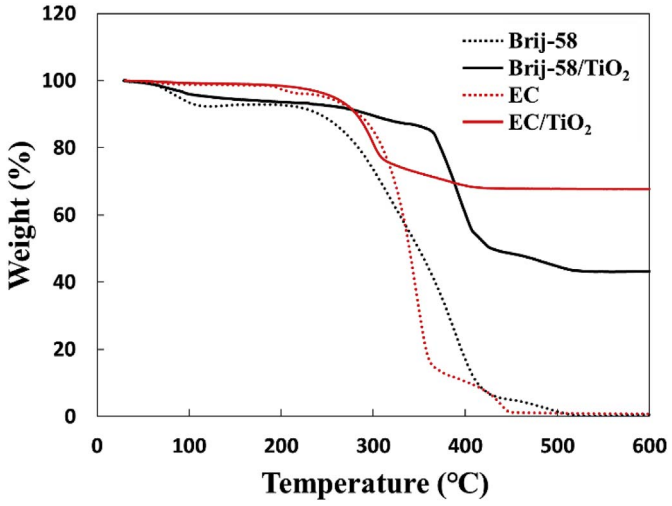

Fig. 3. TGA analyses of Brij-58, EC, Brij-58/TiO_2 NPs, and EC/TiO2 NPs.

molecules can be varied. In addition, we employed EC as another template to create inter-particle porosity for the solid and porous TiO_2 NPs accumulated in the PLs of DSSCs, after which the contributions of both the inter- and intra-particle porosity of the TiO_2 NPs on the photovoltaic performance of the DSSCs were systematically examined.

2. Experimental

Fig. 1a is a schematic of the fabrication of solid and porous TiO_2 NPs using the aerosol-gel chemistry employed in this approach. Briefly, various amounts of Brij-58 surfactant were completely dissolved in distilled water, and then titanium butoxide ($Bi_4Ti_3O_{12}$, TNBT, Sigma-Aldrich) and dilute HCl were added. The molar mixing ratio was TNBT:HCl:Brij-58 = 1:0.004:(0–1), in which the amount of Brij-58 surfactant ($HO(CH_2CH_2O)_{20}C_{16}H_{33}$, Sigma-Aldrich) was varied. The precursor solution was then ultrasonicated for 1 h, and subsequently aerosolized by a standard atomizer operated with filtered compressed air at a pressure of 241 kN m^{-2}. Micrometer-sized droplets containing tiny TiO_2 NPs formed by the aerosol-gel chemistry were generated. The micrometer-sized droplets were then continuously passed through a silica-gel dryer, in which solidified particles were formed through the evaporation and adsorption of the solvent. The resulting particles, composed of either TiO_2 or Brij-58/TiO_2, were then immobilized and sintered by continuously passing them through a quartz-tube reactor (2.54 cm in diameter × 30 cm in heating length) enclosed by a tube furnace heated to around 500 °C. Finally, the resulting TiO_2 or Brij-58/TiO_2 composite NPs were collected on the surface of a membrane filter with a pore size of 200 nm, after which they were calcined at around 500 °C for 1 h to thermally remove the Brij-58 surfactant templates. Fig. 1b shows how the EC templates were added to the TiO_2 NP paste, after which they were calcined at around 500 °C for 30 min to thermally remove the EC to fabricate the TiO_2 NP-accumulated thin film with inter-particle porosity. Both the Brij-58 and EC surfactant templates inside the TiO_2 matrix were expected to prevent the thermal shrinkage of TiO_2 NPs, thus playing a key role in the securing of the pore structures before thermally removing the surfactant.

We fabricated four different types of PLs for DSSCs to systematically examine the effect of various PL structures with inter- and intra-particle porosity of TiO_2 NPs on the photovoltaic performance of the DSSCs. The four different types of DSSCs are shown in Fig. 2: (a) solid PL with solid TiO_2 NPs (Type A), (b) solid PL with porous TiO_2 NPs (Type B; intra-particle porosity), (c) porous PL with solid TiO_2 NPs (Type C; inter-particle porosity) and (d) porous PL with porous TiO_2 NPs (Type D; both inter- and intra-particle porosity). TiO_2 NP-accumulated thin film, which acted as a PL, was formed by a screen-printing process on a fluorine-doped tin oxide (FTO) glass substrate (Pilkington, SnO_2:F, 7 Ω·sq^{-1}) with an active area of 0.6 × 0.6 cm^2. To prepare the TiO_2 paste for the screen-printing process, 0.3 g of TiO_2 NPs, 0.5 mL of acetic acid, 1 g of terpinol, and 0.15 g of EC were mixed into 3 mL of ethanol

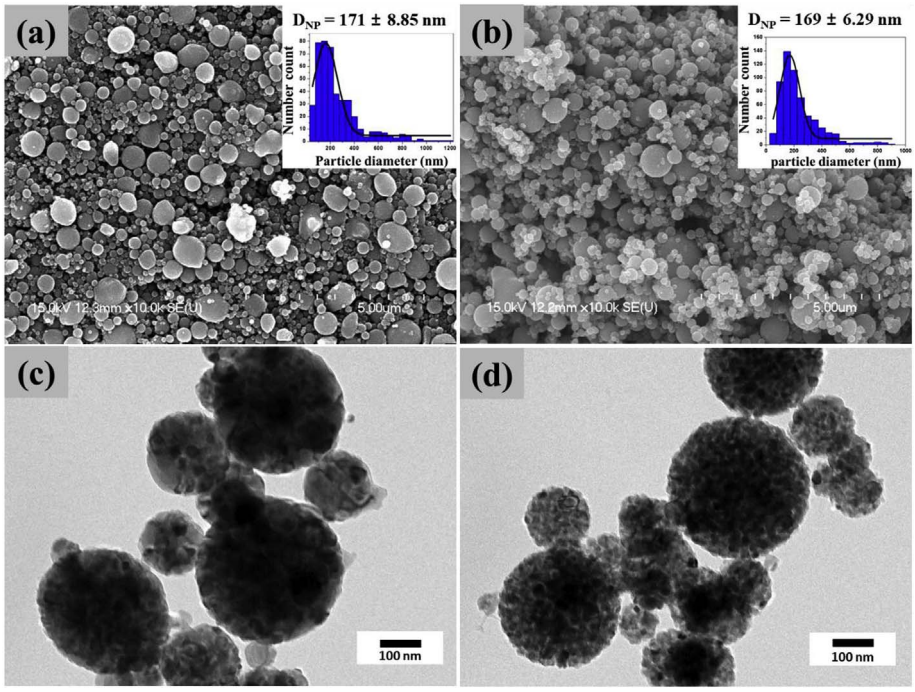

Fig. 4. SEM and TEM images of (a, c) solid TiO_2 NPs before Brij-58 removal and (b, d) porous TiO_2 NPs after Brij-58 removal by calcination process at around 500 °C.

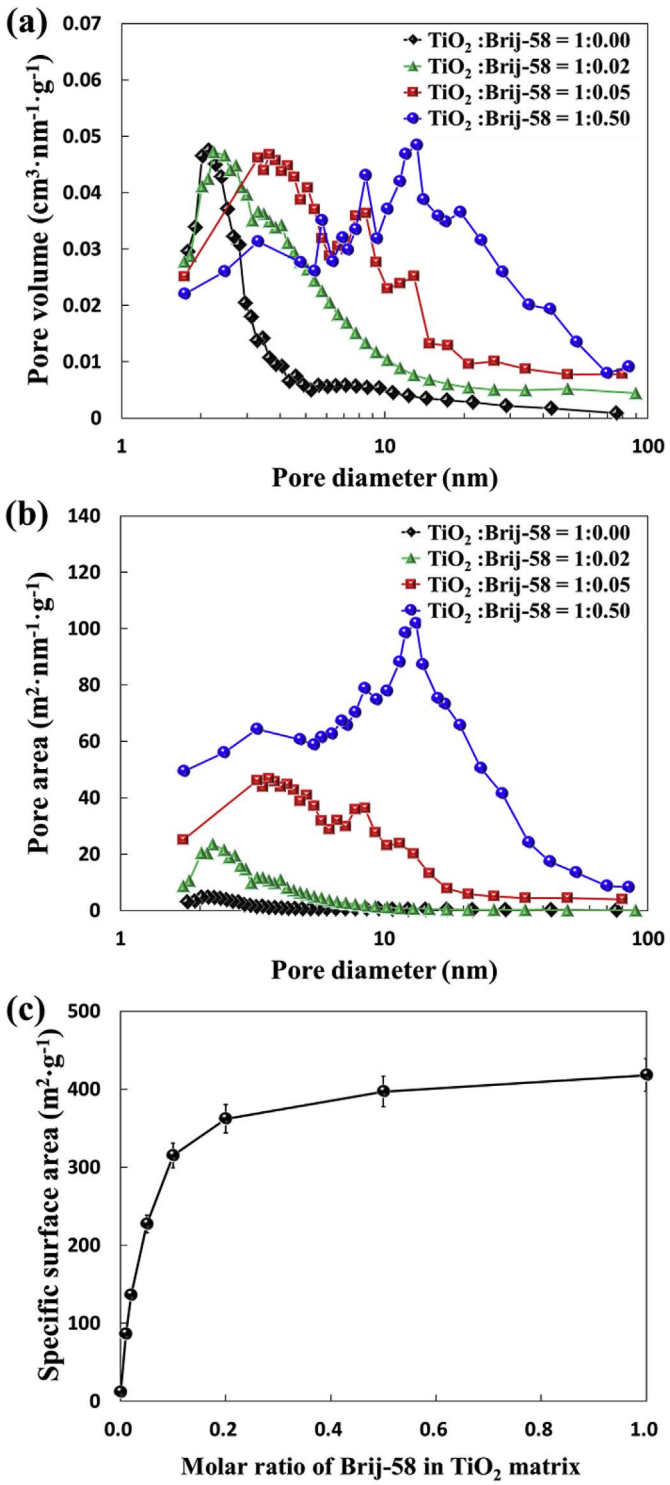

Fig. 5. (a) Pore volume distributions of solid and porous TiO_2 NPs, (b) pore area distributions of solid and porous TiO_2 NPs, and (c) evolution of specific surface area of TiO_2 NPs by varying the amount of Brij-58 added to the TiO_2 matrix.

(EtOH).

The TiO_2 NP-accumulated thin film formed on the FTO glass by the screen-printing process was rapidly dipped into $TiOCl_2$ solution and then sintered at 500 °C for 30 min, and then dye molecules were applied by an electrospray process using anhydrous ethanol containing 0.3-mM Ru-dye $(Bu_4N)_2[Ru(Hdcbpy)_2\text{-}(NCS)_2]$ (N719 dye, Solaronix) for 3 h at 40 °C. This allowed the dye molecules to attach to the entire surface and available inner pores of the solid and porous TiO_2 NPs [23]. The dye-coated TiO_2 NP-accumulated PL was then rinsed with ethanol, after which it was dried in a convection oven at 80 °C for 10 min. For the counter electrode, we prepared Pt-coated FTO glass using an ion sputter (Nasco, HRC 705) operating at 1.2 kV and 7 mA. The dye-coated TiO_2 photoelectrode and Pt-coated counter electrode were sealed together using an inserted hot-melt polymer film (60 μm thick, Surlyn, DuPont), after which an iodide-based liquid electrolyte (Solaronix, AN-50) was injected into the space between the electrodes.

The morphology, SSA, and pore volume distribution of the TiO_2 NPs fabricated by the aerosol-gel and subsequent calcination processes employed in this study were characterized using various techniques, including scanning electron microscopy (SEM, Hitachi, S-4200) operating at around 15 kV, transmission electron microscopy (TEM, JEOL, JEM 2100F) operating at around 100 kV, and a nitrogen gas adsorption technique (BET, Quantachrome, Quadrasorb SI). To evaluate the amount of dye adsorbed, the dye molecules were first desorbed from the TiO_2 NP-accumulated PL by rinsing with a 0.1-M aqueous NaOH solution (i.e., H_2O:EtOH = 1:1). Then, the light absorbance of the dye-containing solution was measured using a Scan UV–Vis spectrophotometer (VARIAN, INC., CARY® 5000) [24–26]. The photocurrent density–voltage (*J–V*) curve and electrochemical impedance spectra (EIS) were automatically recorded using a Keithley SMU 2400 source meter (Cleveland, OH, USA) over a frequency range of 0.1–100 kHz using an open voltage with a pulse of amplitude 10 mV. The intensity of the illumination was calibrated using a standard Si photodiode detector with a KG-5 filter. The incident photon-to-electron conversion efficiency (IPCE) was characterized using a solar simulator (Sun 2000, Abet Technologies Inc., USA) with an arc lamp light source (LS-150-Xe, Abet Technologies Inc., USA) that provided illumination with a wavelength of between 300 and 800 nm.

3. Results and discussion

To determine the appropriate calcination temperature for the Brij-58 and EC surfactants added to the TiO_2 NPs, we performed thermogravimetric analyses (TGA), as shown in Fig. 3. We can clearly observe that Brij-58 and EC were completely removed at temperatures > 400 °C. The mass ratios of TiO_2 to Brij-58/TiO_2 and EC/TiO_2 were estimated to be approximately 0.42 and 0.66 (Here, M_{TiO2} = 79.866 g mol^{-1}; $M_{TiO2+Brij\text{-}58}$ = 192.266 g mol^{-1}; $M_{TiO2+EC}$ = 120.772 g mol^{-1}) when the molar ratio of TiO_2: Brij-58 = 1:0.1 and that of TiO_2: EC = 1:0.1, respectively. From this calculation, we expected to be able to obtain the TiO_2 content in the Brij-58/TiO_2 and EC/TiO_2 composite NPs from an approximately 42% and 66% weight change after calcination at > 400 °C, which was clearly observed in Fig. 3.

The formation of solid and porous TiO_2 NPs in the aerosol-gel process employed in the present study was examined by SEM and TEM analyses, as shown in Fig. 4. From the SEM images shown in Fig. 4a and b, the TiO_2 NPs were spherical structures with average diameters of around 171 ± 8.85 nm and around 169 ± 6.29 nm, before and after, respectively, removing the Brij-58 surfactant. This suggests that there were no appreciable changes in the overall structures of the TiO_2 NPs before and after the thermal removal of the Brij-58 surfactant. Fig. 4c and d shows TEM images of the TiO_2 NPs formed before and after the calcination process. Before the calcination process, the Brij-58/TiO_2 composite NPs were found to be solid particles (Fig. 4c). However, after the calcination process, small primary solid TiO_2 spheres formed by the sol-gel process in the aerosolized droplets had clustered into large spherical particles due to the fast sintering. A slight decrease in the electron beam attenuation was observed in the interior of the resulting

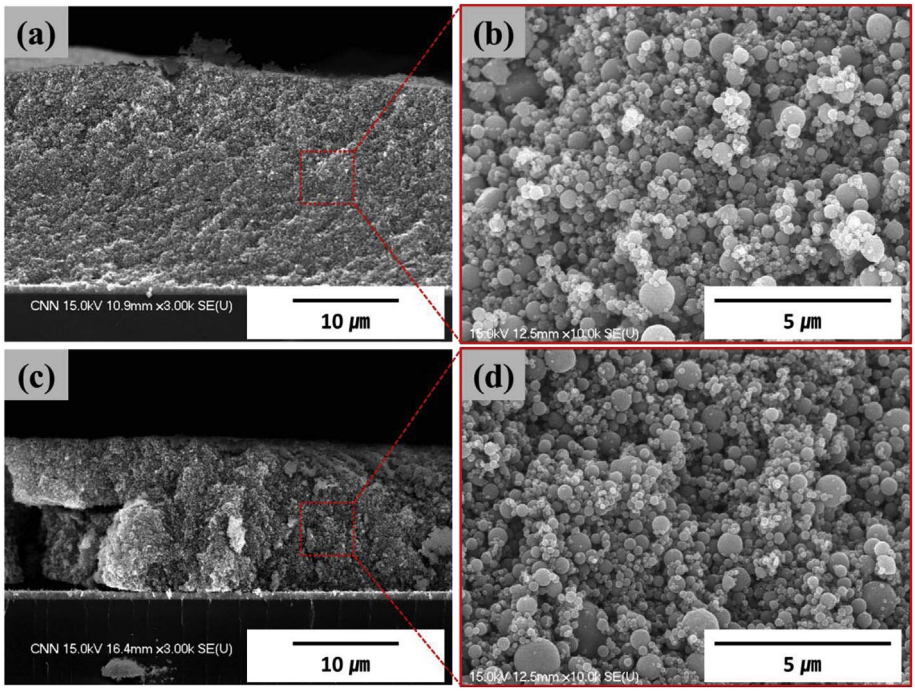

Fig. 6. Cross-sectional SEM images of (a, b) TiO_2 NPs without inter-particle porosity (solid PL) and (c, d) TiO_2 NPs with inter-particle porosity (porous PL).

Table 1
Photovoltaic characteristics of DSSCs fabricated using solid and porous TiO_2 NPs with inter- and intra-particle porosity.

Type of DSSCs	TiO_2:EC	TiO_2:Brij-58	τ_e [ms]	*DA* [10^{-7} mol cm^{-2}]	R_t (Ω)	R_{rec} (Ω)	J_{sc} [mA cm^{-2}]	V_{oc} [V]	*FF*	*PCE* [%]
Type A	1:0.00 (Solid PL)	1:0.00 (Solid NPs)	1.3	0.62	2	36	4.30 ± 0.09	0.69 ± 0.01	0.72 ± 0.01	2.14 ± 0.04
Type B	1:0.00 (Solid PL)	1:0.50 (Porous NPs)	2.0	0.85	2	16	6.33 ± 0.94	0.69 ± 0.01	0.71 ± 0.01	3.10 ± 0.46
Type C	1:0.1 (Porous PL)	1:0.00 (Solid NPs)	2.5	0.93	3	12	8.51 ± 0.80	0.68 ± 0.01	0.73 ± 0.01	4.22 ± 0.27
Type D	1:0.1 (Porous PL)	1:0.50 (Porous NPs)	5.0	2.25	3	8	15.30 ± 0.23	0.67 ± 0.01	0.73 ± 0.01	7.48 ± 0.06

*Type A: solid photoactive layer (PL) with solid TiO_2 nanoparticles (NPs).
Type B: solid PL with porous TiO_2 NPs (intra-particle porosity).
Type C: porous PL with solid TiO_2 NPs (inter-particle porosity).
Type D: porous PL with porous TiO_2 NPs (inter- and intra-particle porosity).
τ_e: electron lifetime, *DA*: dye adsorption, R_t: transport resistance, R_{rec}: recombination resistance. J_{sc}: short-circuit current, V_{oc}: open-circuit voltage, *FF*: fill factor, PCE: power conversion efficiency.

TiO_2 NP after the surfactant had been removed, thus confirming that the Brij-58 surfactant could be presented within the TiO_2 NPs (Fig. 4d).

To observe the effect of the amount of Brij-58 on the pore structures in the resulting TiO_2 NPs, the pore volume distribution and SSA of the TiO_2 NPs were measured using a gas sorptometer (nitrogen adsorption at 77 K using the BET equation) as shown in Fig. 5. The pore volume distributions shown in Fig. 5a were observed to increase with the amount of Brij-58 surfactant in the TiO_2 matrix, suggesting that Brij-58 templates effectively supported the formation of TiO_2 NPs with intra-particle porosity. A relatively large pore area was also obtained, for which the pore sizes ranged from 2 to 100 nm, with a larger pore area being formed as more Brij-58 was used, as shown in Fig. 5b. We can also see that the SSA determined by BET theory for the solid TiO_2 NPs without using Brij-58 was only around 12 $m^2 g^{-1}$. However, it increased significantly to around 86 $m^2 g^{-1}$ for TiO_2:Brij-58 = 1:0.01, around 227 $m^2 g^{-1}$ for TiO_2:Brij-58 = 1:0.05, around 362 $m^2 g^{-1}$ for TiO_2:Brij-58 = 1:0.2, and then almost saturated at around 418 $m^2 g^{-1}$ for TiO_2: Brij-58 = 1:1, as shown in Fig. 5c. This suggests that the Brij-58 surfactant is a very effective templating medium for creating controlled pore structures in TiO_2 matrices. In addition, to examine the role of EC on the formation of inter-particle porosity, cross-sectional views of solid PL (Type A) and porous PL (Type C) were observed using SEM as shown in Fig. 6. In the case of solid PLs without using an EC template, the interspace formed between the TiO_2 NPs was seemed to be very narrow and the TiO_2 NPs had densely accumulated (Fig. 6a and b). However, in the case of porous PLs, larger inter-particle pore structures and craters were easily observed after removing the EC templates (Fig. 6c and d). This also suggests that the EC templates effectively created inter-particle porosity between the TiO_2 NPs in the PLs.

To examine the effect of the inter- and intra-particle porosity of TiO_2 NPs on the photovoltaic performance of DSSCs, we assembled DSSCs with four different PLs stacked with the solid and porous TiO_2 NPs fabricated in the present study. Again, EC was employed to create inter-particle porosity in the TiO_2 NPs accumulated in the PLs using a screen-

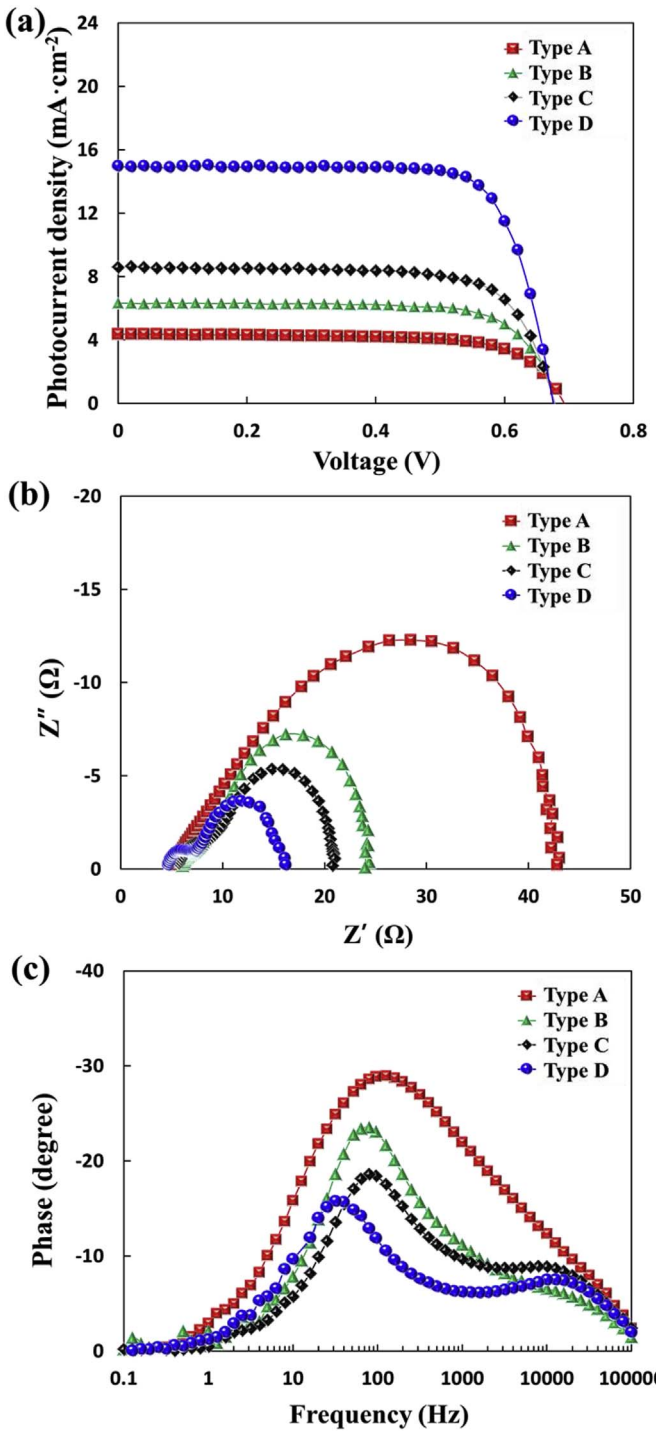

Fig. 7. (a) Photocurrent density–voltage (*J–V*) curves, (b) Nyquist plots, and (c) Bode plots for different types of DSSCs with inter- and intra-particle porosity.

printing process, and Brij-58 was employed to create intra-particle porosity in the TiO_2 NPs fabricated using the aerosol-gel and subsequent calcination processes. Table 1 and Fig. 7 summarize the levels of photovoltaic performance of the DSSCs with four different PL structures. Without either inter- or intra-particle porosity of the TiO_2 (Type A), the resulting PCE of DSSC was only around 2.14% owing to the extremely low dye adsorption ($DA = \sim 0.62 \times 10^{-7}$ mol cm^{-2}).

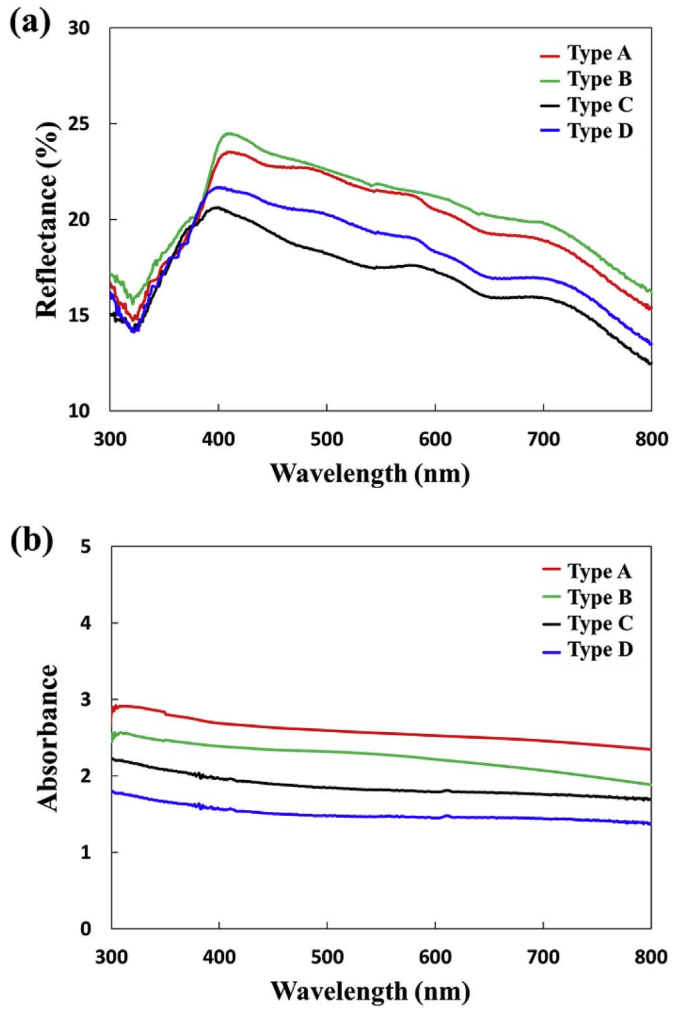

Fig. 8. UV–vis spectrometer measurements of reflectance and absorbance spectra for different types of DSSCs with inter- and intra-particle porosity.

However, when porous TiO_2 NPs with intra-particle porosity were accumulated in the solid PL (Type B), the PCE of the DSSCs was increased up to around 3.10%, which was a result of the increased dye adsorption ($DA = \sim 0.85 \times 10^{-7}$ mol cm^{-2}). It is interesting to note that the amount of dye adsorption and the PCE of the DSSC were greatly increased in the case of Type C (i.e., $DA = \sim 0.93 \times 10^{-7}$ mol cm^{-2}, PCE = ~4.22%), relative to Type B. Here, Type C is a DSSC composed of porous PLs which are accumulated with solid TiO_2 NPs so that there is a relatively high inter-particle porosity. This suggests that the inter-particle porosity of the solid TiO_2 NPs is much more effective at supporting more dye molecules than the intra-particle porosity of porous TiO_2 NPs. When we examined the porous PLs with porous TiO_2 NPs (Type D), the resulting PCE of the DSSC reached a maximum value of around 7.48% owing to considerably increased dye adsorption ($DA = \sim 2.25 \times 10^{-7}$ mol cm^{-2}). V_{oc} for all the DSSCs did not change appreciably. However, *FF* increased slightly when Types C and D were compared with Types A and B. *FF* is known to be inversely proportional to the internal resistances of the DSSCs. In the cases of those DSSCs with solid PLs for Type A and B, their recombination resistances (R_{rec}) measured were found to be much higher than those of Type C and D with the porous PLs, as shown in Table 1.

Another possible reason for the higher *FF* and lower internal

Table 2
Photovoltaic characteristics of DSSCs fabricated using porous TiO_2 NPs formed with different ratios of Brij-58 and TiO_2.

Type of DSSCs	TiO_2:Brij-58	τ_e [ms]	*DA* [10^{-7} mol cm^{-2}]	*SSA* of TiO_2 NPs [m^2·g^{-1}]	*APS* of TiO_2 NPs [nm]	J_{sc} [mA cm^{-2}]	V_{oc} [V]	*FF*	*PCE* [%]
Type D	1:0.01	2.0	0.95	86	4.9	9.40 ± 0.04	0.69 ± 0.01	0.74 ± 0.01	4.80 ± 0.06
	1:0.02	2.5	1.12	136	6,1	11.71 ± 0.27	0.67 ± 0.01	0.72 ± 0.01	5.64 ± 0.24
	1:0.05	3.1	1.25	227	7.4	12.13 ± 0.09	0.67 ± 0.01	0.74 ± 0.01	6.01 ± 0.03
	1:0.10	3.1	1.31	350	9.9	12.25 ± 0.15	0.67 ± 0.01	0.74 ± 0.01	6.07 ± 0.05
	1:0.20	4.0	1.98	362	13.3	13.65 ± 0.08	0.68 ± 0.01	072 ± 0.01	6.68 ± 0.07
	1:0.50	5.0	2.24	397	14.2	15.30 ± 0.23	0.67 ± 0.01	0.73 ± 0.01	7.48 ± 0.06
	1:1.00	5.0	2.25	418	15.6	14.90 ± 0.12	0.68 ± 0.01	0.75 ± 0.01	7.60 ± 0.09

*Type D: porous photoactive layer with porous TiO_2 NPs, PL: photoactive layer, τ_e: electron lifetime, *DA*: dye adsorption, *SSA*: specific surface area, *APS*: average pore size, J_{sc}: short-circuit current, V_{oc}: open-circuit voltage, *FF*: fill factor, PCE: power conversion efficiency.

resistance of Types C and D with the porous PLs, relative to Types A and B with the solid PLs, can be inferred from the inherently better light harvesting. This was corroborated by examining the spectroscopic properties of solid and porous PLs with the assistance of UV–Vis reflectance and absorbance spectra analyses, as shown in Fig. 8. The reflectance of solid photoactive layer (PL) with porous TiO_2 NPs (Type B) in a spectral range of 300–800 nm was higher than that of solid PL with solid TiO_2 NPs (Type A). However, the absorbance of solid PL with porous TiO_2 NPs (Type B) was lower than that of solid PL with solid TiO_2 nanoparticles (Type A). This suggests that the porous TiO_2 NPs fabricated in the present study played an important role of light scattering medium as well as dye adsorption sites. Furthermore, the magnitudes of the reflectance and absorbance of the solid PLs (Types A and B) were observed to be much higher than those of the porous PLs (Types C and D). This suggests that the solid PLs strongly reflected and absorbed the incident light, such that it could not effectively pass through the solid PLs. However, the porous PLs allowed more incident light to pass through the inter-particle pores, implying that light harvesting can be effectively achieved by tuning the inter-particle porosity of the TiO_2 NPs in the PLs of DSSCs.

The synergistic effects of the inter- and intra-particle porosity of TiO_2 NPs on the photovoltaic performance of DSSCs were clearly identified. We need to further investigate how the evolution of intra-particle porosity can affect the resulting PCE of DSSCs. Table 2 summarizes the amount of dye adsorption in the porous PLs stacked with porous TiO_2 NPs in the case of Type D (i.e., both inter- and intra-particle porosity), the SSA of porous TiO_2 NPs, and the photovoltaic performance of the DSSCs. It is clear that the SSA and the amount of dye adsorbed by the porous TiO_2 NPs increased with the amount of Brij-58 in the TiO_2 NPs. Both the SSA and amount of dye adsorption increased significantly with the addition of relatively small amounts of Brij-58 (i.e., TiO_2:Brij-58 = 1:(0.01–0.1)), and they seemed to saturate at their maximum values with the addition of larger amounts of Brij-58 (i.e., TiO_2:Brij-58 = 1:(0.2–1)).

Fig. 9 shows the *J–V* curves and electrochemical impedance spectroscope (EIS) measurements for the fabricated DSSCs, measured under AM 1.5 illumination (100 mW cm^{-2}) as a function of the molar fractions of Brij-58 presented in the Brij-58/TiO_2 composite NPs. For different molar ratios of Brij-58 in the Brij-58/TiO_2 NPs, J_{sc} increased with the molar ratio of Brij-58 in the porous TiO_2 NP-based PLs of the DSSCs. The J_{sc} values of the DSSCs composed of porous TiO_2 NPs increased from 9.40 ± 0.04 mA cm^{-2} for TiO_2: Brij-58 = 1:0.01 to 15.30 ± 0.23 mA cm^{-2} for TiO_2:Brij-58 = 1:0.5, resulting in a considerable improvement of the PCE from 4.80 ± 0.06% to 7.48 ± 0.06%, respectively. This increase in the photovoltaic performance using the porous TiO_2 NPs occurred because of the relatively high SSA and sufficiently large pore size in the case of the porous TiO_2 NPs, which enabled the adsorption of a larger number of dye molecules; this was a major factor responsible for improving both the J_{sc} and PCE values of the DSSCs. However, note that both the V_{oc} and *FF* of the DSSCs fabricated with the porous TiO_2 NPs did not exhibit any appreciable changes, even in comparison with those of the DSSCs fabricated with the solid TiO_2 NPs. This suggests that the photovoltaic properties of the solid and porous TiO_2 NPs were very similar. EIS measurements were also carried out to identify the charge transfer-related internal resistance of the porous TiO_2 NPs fabricated in this study, as shown in Fig. 9b and c. The Nyquist plots in Fig. 9b show that the porous TiO_2 NPs with the higher SSA reduced the charge transfer resistance at the TiO_2 NP/dye/electrolyte interfaces. The porous TiO_2 NPs with the higher SSA can absorb more dye molecules and generate more electrons in the DSSCs, which eventually results in a lower resistance and higher J_{sc}. Fig. 9c shows Bode phase plots for analyzing the electron lifetime. The maximum frequency decreased as the molar ratio of Brij-58 in the TiO_2 NPs was increased, and the electron lifetime ($\tau_e = [2\pi f_{max}]^{-1}$, where f_{max} is the maximum frequency [27]) increased from around 2.0 ms for TiO_2:Brij-58 = 1:0.01 to around 5.0 ms for TiO_2:Brij-58 = 1:0.5, suggesting that the photogenerated electrons diffuse further owing to the more open porous TiO_2 structure.

To understand the major factors leading to the improvement in PCE in porous TiO_2 NP-based DSSCs, the incident photon-to-electron conversion efficiency (IPCE) spectra were measured as a function of the incident light wavelength. The IPCE spectra shown in Fig. 10 show that the porous PLs stacked with porous TiO_2 NP-based DSSCs with a higher molar ratio of Brij-58 exhibited a better IPCE than the those with a lower molar ratio of Brij-58, suggesting that the porous TiO_2 NPs with a higher molar ratio of Brij-58 support more dye molecules so that they can generate more electrons when irradiated by sunlight. This confirms that the porous PLs stacked with highly porous TiO_2 NPs are a very effective dye-supporting medium capable of enhancing the photovoltaic performance of DSSCs.

4. Conclusions

We fabricated surfactant-templated TiO_2 NPs with inter- and intra-particle porosity. First, with the assistance of Brij-58-templated aerosol-gel and subsequent calcination processes, porous TiO_2 NPs with intra-particle porosity were fabricated. By varying the amount of Brij-58 added to the TiO_2 matrix, the pore size and volume of the fabricated TiO_2 NPs was successfully controlled. Second, EC was employed as another templating medium, and then a TiO_2 NP-accumulated thin film

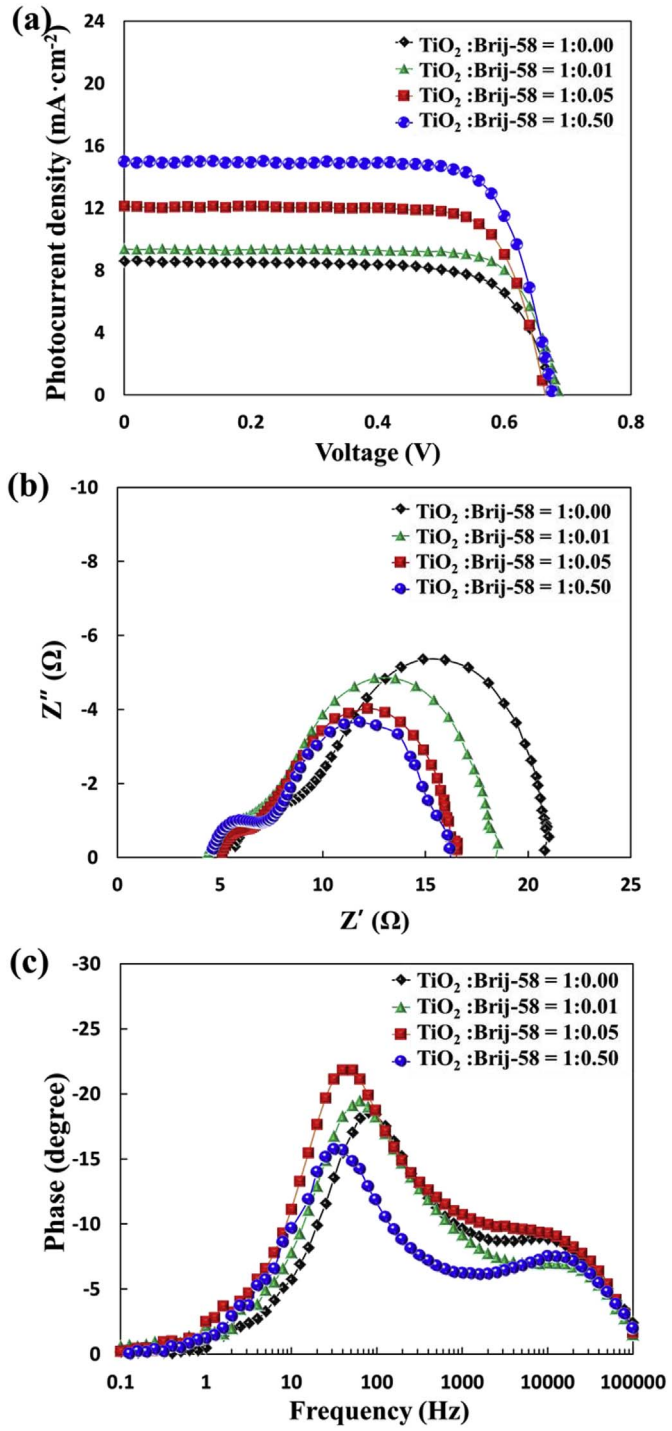

Fig. 9. (a) Photocurrent density–voltage (*J–V*) curves, (b) Nyquist plots, and (c) Bode plots for different types of DSSCs with porous PLs stacked with porous TiO_2 NPs, which was controlled by varying the ratios of the TiO_2 and Brij-58.

with inter-particle porosity was successfully fabricated using screen printing after the calcination process. As a result, the photovoltaic performance of the DSSCs with inter-particle porosity was much better than that of the DSSCs with intra-particle porosity owing to the extra dye adsorption, suggesting that the control of dye adsorption with the inter-particle porosity of TiO_2 NPs is much more effective than dye adsorption with the intra-particle porosity of TiO_2 NPs. Finally, the DSSCs with inter- and intra-particle porosity was found to have the best photovoltaic performance because it could take advantage of the synergistic effects of the inter- and intra-particle porosity of the TiO_2 NPs

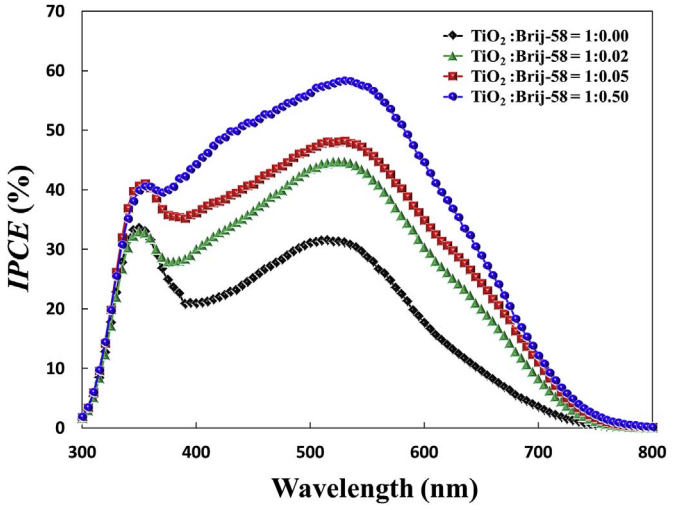

Fig. 10. IPCE spectra of different DSSCs with porous PLs stacked with porous TiO_2 NPs, which was controlled by varying the ratios of the TiO_2 and Brij-58.

so that the enhanced SSA of the TiO_2 NPs could support relatively large amounts of dye molecules. Simultaneously, the porous structures of the TiO_2 NPs inherently allowed light to pass easily through the PLs, thus significantly promoting light harvesting. This suggests that tuning the inter- and intra-particle porosity of the TiO_2 NPs accumulated in the PLs would be a very effective strategy for enhancing the photovoltaic performance of DSSCs.

Conflicts of interest

There are no conflicts of interest to declare.

Acknowledgements

This research was supported by Basic Science Research Programs through the National Research Foundation of Korea (NRF) funded by the Ministry of Science and ICT and Ministry of Education (No. 2015R1A2A1A15054036 & 2016R1A6A3A11932418).

Appendix A. Supplementary data

Supplementary data related to this article can be found at http://dx.doi.org/10.1016/j.micromeso.2018.03.003.

References

[1] M. Grätzel, Dye-sensitized solar cells, J. Photochem. Photobiol. C 4 (2003) 145.
[2] M. Ikegami, J. Suzuki, K. Teshima, M. Kawaraya, T. Miyasaka, Improvement in durability of flexible plastic dye-sensitized solar cell modules, Sol. Energy Mater. Sol. Cells 93 (2009) 836.
[3] T. Yamaguchi, Y. Uchida, S. Agatsuma, H. Arakawa, Series-connected tandem dye-sensitized solar cell for improving efficiency to more than 10%, Sol. Energy Mater. Sol. Cells 216 (2010) 104.
[4] R. Katoh, M. Kasuya, A. Furube, N. Fuke, N. Koide, L. Han, Quantitative study of solvent effects on electron injection efficiency for black-dye-sensitized nano crystalline TiO_2 films, Sol. Energy Mater. Sol. Cells 93 (2009) 698.
[5] A.B. Rudine, N.U. Day, X. Tian, C. Lee, K.E. James, C.C. Wamser, Aminophenyl/carboxyphenylporphyrins as sensitizers for dye-sensitized solar cells, J. Porphyr. Phthalocyanines 20 (2016) 1217.
[6] Q. Ma, Y. Cui, X. Deng, X. Chen, Q. Cheng, B. Li, Controllable fabrication of TiO_2 nanobelts/nanotubes photoelectrode for dye-sensitized solar cells, J. Nanosci. Nanotechnol. 17 (2017) 2072.
[7] J.H. Pan, X.S. Zhao, I.L. Wan, Block copolymer-templated synthesis of highly organized mesoporous TiO_2-based films and their photoelectrochemical applications, Chem. Eng. J. 170 (2011) 363.
[8] Y. Iu, X. Sun, Q. Tai, H. Hu, B. Chen, N. Huang, B. Sebo, X.Z. Zhao, Efficiency enhancement in dye-sensitized solar cells by interfacial modification of con-ducting glass/mesoporous TiO_2 using a novel ZnO compact blocking film, J. Power Sources 196 (2011) 475.

[9] X. Luo, J.Y. Ahn, Y.S. Park, J.M. Kim, H.W. Lee, S.H. Kim, Rapid fabrication and photovoltaic performance of pt-free carbon nanotube counter electrodes of dye-sensitized solar cells, Sol. Energy 150 (2017) 13.
[10] P. Chen, C. Li, C. Lee, R. Vittal, K. Ho, PEDOT-decorated nitrogen-doped graphene as the transparent composite film for the counter electrode of a dye-sensitized solar cell, Nano Energy 12 (2015) 374.
[11] D.H. Chen, L. Cao, F.Z. Huang, P. Imperia, Y.B. Cheng, R.A. Caruso, Synthesis of monodisperse mesoporous titania beads with controllable diameter, high surface areas, and variable pore diameters (14–23 nm), J. Am. Chem. Soc. 132 (2010) 4438.
[12] D.H. Chen, F.Z. Huang, Y.B. Cheng, R.A. Caruso, Mesoporous anatase TiO_2 beads with high surface areas and controllable pore sizes: a superior candidate for high-performance dye-sensitized solar cells, Adv. Mater. 21 (2009) 2206.
[13] F.Z. Huang, D.H. Chen, X.L. Zhang, R.A. Caruso, Y.B. Cheng, Dual-function scattering layer of submicrometer-sized mesoporous TiO_2 beads for high-efficiency dye-sensitized solar cells, Adv. Funct. Mater. 20 (2010) 1301.
[14] F. Sauvage, D.H. Chen, P. Comte, F.Z. Huang, L.P. Heiniger, Y.B. Cheng, R.A. Caruso, M. Graetzel, Dye-sensitized solar cells employing a single film of mesoporous TiO_2 beads achieve power conversion efficiencies over 10%, ACS Nano 4 (2010) 4420.
[15] Y.J. Kim, M.H. Lee, H.J. Kim, G. Lim, Y.S. Choi, N.G. Park, K. Kim, W.I. Lee, Formation of highly efficient dye-sensitized solar cells by hierarchical pore generation with nanoporous TiO_2 spheres, Adv. Mater. 21 (2009) 1.
[16] W.G. Yang, F.R. Wan, Q.W. Chen, J.J. Li, D.S. Xu, Controlling synthesis of well-crystallized mesoporous TiO_2 microspheres with ultrahigh surface area for high-performance dye-sensitized solar cells, J. Mater. Chem. 20 (2010) 2870.
[17] A.I. Maldonado-Valdivia, E.G. Galindo, M.J. Ariza, M.J. García-Salinas, Surfactant influence in the performance of titanium dioxide photoelectrodes for dye-sensitized solar cells, Sol. Energy 91 (2013) 263.
[18] H.Y. Byun, R. Vittal, D.Y. Kim, K.J. Kim, Beneficial role of cetyltrimethylammonium Bromide in the enhancement of photovoltaic properties of dye-sensitized rutile TiO_2 solar cells, Langmuir 20 (2004) 6853.
[19] A. Latini, R. Panetta, C. Cavallo, D. Gozzi, S. Quaranta, A comparison of the performances of different mesoporous titanias in dye-sensitized solar cells, J. Nanomater. 2015 (2015) 450405.
[20] L. Hu, S. Dai, J. Weng, S. Xiao, Y. Sui, Y. Huang, S. Chen, F. Kong, X. Pan, L. Liang, K. Wang, Microstructure design of nanoporous TiO_2 photoelectrodes for dye-sensitized solar cell modules, J. Phys. Chem. B 111 (2007) 358.
[21] S. Ito, T.N. Murakami, P. Comte, P. Liska, C. Grätzel, M.K. Nazeeruddin, M. Grätzel, Fabrication of thin film dye sensitized solar cells with solar to electric power conversion efficiency over 10%, Thin Solid Films 516 (2008) 4613.
[22] F. Sauvage, D. Chen, P. Comte, F. Huang, L. Heiniger, Y. Cheng, R.A. Caruso, M. Graetzel, Dye-sensitized solar cells employing a single film of mesoporous TiO_2 beads achieve power conversion efficiencies over 10%, ACS Nano 4 (2010) 4420.
[23] X. Luo, J.H. Kim, J.Y. Ahn, D.Y. Lee, J.M. Kim, D. Lee, S.H. Kim, Electrospraying-assisted rapid dye molecule uptake on the surfaces of TiO_2 nanoparticles for speeding up dye-sensitized solar cell fabrication, Sol. Energy Mater. Sol. Cells 144 (2016) 411.
[24] H.J. Koo, Y.J. Kim, Y.H. Lee, W.I. Lee, K. Kim, N.G. Park, Nano-embossed hollow spherical TiO_2 as bifunctional material for high-efficiency dye-sensitized solar cells, Adv. Mater. 20 (2008) 195.
[25] J.Y. Ahn, J.H. Kim, K.J. Moon, S.D. Park, S.H. Kim, Synergistic effects of the aspect ratio of TiO_2 nanowires and multi-walled carbon nanotube embedment for enhancing photovoltaic performance of dye-sensitized solar cells, Nanoscale 5 (2013) 6842.
[26] J.Y. Ahn, K.J. Moon, J.H. Kim, S.H. Lee, J.W. Kang, H.W. Lee, S.H. Kim, Designed synthesis and stacking architecture of solid and mesoporous TiO_2 nanoparticles for enhancing the light-harvesting efficiency of dye-sensitized solar cells, ACS Appl. Mater. Interfaces 6 (2014) 903.
[27] J. Qian, P. Liu, Y. Xiao, Y. Jiang, Y. Cao, X. Ai, H. Yang, TiO_2-coated multilayered SnO_2 hollow microspheres for dye-sensitized solar cells, Adv. Mater. 21 (2009) 3663.